

TESTING THE ISOTROPY OF HIGH ENERGY COSMIC RAYS USING SPHERICAL NEEDLETS

BY GILLES FAÏ, JACQUES DELABROUILLE,
GÉRARD KERKYACHARIAN AND DOMINIQUE PICARD

*Ecole Centrale Paris, CNRS and Université Paris Diderot,
Université Paris Diderot and Université Paris Diderot*

For many decades, ultrahigh energy charged particles of unknown origin that can be observed from the ground have been a puzzle for particle physicists and astrophysicists. As an attempt to discriminate among several possible production scenarios, astrophysicists try to test the statistical isotropy of the directions of arrival of these cosmic rays. At the highest energies, they are supposed to point toward their sources with good accuracy. However, the observations are so rare that testing the distribution of such samples of directional data on the sphere is nontrivial. In this paper, we choose a non-parametric framework that makes weak hypotheses on the alternative distributions and allows in turn to detect various and possibly unexpected forms of anisotropy. We explore two particular procedures. Both are derived from fitting the empirical distribution with wavelet expansions of densities. We use the wavelet frame introduced by [*SIAM J. Math. Anal.* **38** (2006b) 574–594 (electronic)], the so-called needlelets. The expansions are truncated at scale indices no larger than some J^* , and the L^p distances between those estimates and the null density are computed. One family of tests (called MULTIPLE) is based on the idea of testing the distance from the null for each choice of $J = 1, \dots, J^*$, whereas the so-called PLUGIN approach is based on the single full J^* expansion, but with thresholded wavelet coefficients. We describe the practical implementation of these two procedures and compare them to other methods in the literature. As alternatives to isotropy, we consider both very simple toy models and more realistic nonisotropic models based on Physics-inspired simulations. The Monte Carlo study shows good performance of the MULTIPLE test, even at moderate sample size, for a wide sample of alternative hypotheses and for different choices of the parameter J^* . On the 69 most energetic events published by the Pierre Auger Collaboration, the needlelet-based procedures suggest statistical evidence for anisotropy. Using several values for the parameters of the methods, our procedures yield p -values below 1%, but with uncontrolled multiplicity issues. The flexibility of this method and the possibility to modify it to take into account a large variety of extensions of the problem make it an interesting option for future investigation of the origin of ultrahigh energy cosmic rays.

Received July 2011; revised December 2012.

Key words and phrases. Nonparametric test, isotropy test, multiple tests, ultrahigh energy cosmic rays, wavelet procedure.

1. Introduction.

1.1. *Motivation.* It is a common problem in astrophysics to analyse data sets containing measurements of a number of objects (such as galaxies of a particular type) or of events (such as cosmic rays or gamma ray bursts) distributed on the celestial sphere. Each set of such objects or events can be represented as a collection of positions $X_i = (\theta_i, \phi_i)$, $i = 1, \dots, n$, in \mathbb{S} the unit sphere of \mathbb{R}^3 . In many cases, such objects trace an underlying probability distribution f on the sphere, which itself depends on the physics which governs the production of the objects and events. Galaxies, for instance, form in over-densities of a preexisting smooth field of distribution of matter in the universe, and the study of the statistics of their distribution has grown into a field of astrophysics by itself [Martínez and Saar (2002)].

The case of ultrahigh energy cosmic rays (UHECRs) is of particular interest, and is the main focus of the present work. UHECRs are particles of unknown origin which arrive at the Earth from apparently random directions of the sky. These particles interact with atoms of the upper atmosphere, generating a huge cascade of billions of secondary particles. The observation of these secondary particles with appropriate detectors on ground permits the measurement of the direction of arrival and of the energy of the original cosmic ray.

The existence of cosmic rays has been known for about a century. Such particles exist with a very wide range of kinetic energies, from few eV to more than 10^{20} eV.¹ Observed cosmic rays are typically ordinary charged particles (electrons, protons and nuclei), propagating in empty space, and deflected by galactic magnetic fields. The rate of observed cosmic rays in the vicinity of the Earth, however, decreases rapidly with energy. At low energy, the observed cosmic rays are numerous and their composition is well known. There also exist several known astrophysical processes responsible for their acceleration, such as stellar winds for the least energetic ones, to violent phenomena such as supernovae shock waves at higher energy. At the highest energies ($E \geq 10^{20}$ eV), however, the observed flux is of the order of 1 event per square kilometre per century, which limits the statistics of observed events to few tens of events (in two decades of observations). In addition, no understood astrophysical process, involving known objects, can accelerate particles to such tremendous energies.

Recent observations of ultrahigh energy cosmic rays suggest that they are ordinary particles, such as protons and nuclei, accelerated in extremely violent astrophysical phenomena [see Kotera and Olinto (2011), for a recent review on the astrophysics of UHECRs]. However, many alternate hypotheses concerning their nature and origin have been proposed over the years [see, e.g., Hillas (1984), Torres and Anchordoqui (2004), Cronin (2005)]. UHECRs could originate from active

¹1 eV = 1 electron Volt $\simeq 1.6 \times 10^{-19}$ Joule.

galactic nuclei (AGN), or from neutron stars surrounded by extremely high magnetic fields, or yet from many other processes. It is also possible that the type and origin of ultrahigh energy cosmic rays (at energies above 10^{19} eV) depend, at least to some extent, upon the energy at which they are observed. Indeed, the most energetic cosmic rays cannot propagate very far (i.e., not much more than ~ 100 Mpc) without losing most of their energy by interactions with photons from the Cosmic Microwave Background [the so-called GZK effect; Greisen (1966), Zatsepin and Kuz'min (1966)]. The confirmation of the energy cutoff at the high end of the cosmic ray spectrum is one of the main achievements of the Pierre Auger Observatory [Abraham et al. (2008, 2010b)].

Before the location and physical process of acceleration have been clearly identified, taking into account the fact that most of the evidence about the chemical composition of cosmic rays at the highest energies rely on extrapolations of the present knowledge of hadronic interactions at energies two orders of magnitude above the range presently tested at the LHC, it is difficult to completely rule out alternate theoretical explanations as to what UHECRs exactly are and what is their origin. Alternate hypotheses such as production by decay of long-lived relic particles from the Big Bang, about 13 billion years old [Bhattacharjee and Sigl (2000)], are just starting to be disfavored by the observations of the Pierre Auger collaboration, with recently published results about primary photon limits that impose stringent limits on these kinds of models [Pierre Auger Collaboration (2009)].

In an attempt to better understand the origin of such UHECRs, physicists study the statistical distribution of their directions of arrival, looking for two particular signatures. First, the (statistically significant) arrival of more than one UHECR from the same direction on the sky would indicate that their production is not likely to originate from single time events (e.g., catastrophic mergers of two compact astrophysical objects), but rather from sources which emit UHECRs regularly.² Second, one may look for correlation in the directions of arrival of UHECRs with known astrophysical objects, as nearby active galactic nuclei, in an attempt to identify plausible production sites. Hence, in some hypotheses, the underlying probability distribution for the directions of incidences of observed UHECRs would be a finite sum of point-like sources—or nearly point-like, taking into account the deflection of the cosmic rays by magnetic fields. In other hypotheses, the distribution could be uniform, or smooth and correlated with the local distribution of matter in the universe. The distribution could also be a superposition of the above. Distinguishing between these hypotheses is of primordial importance for understanding the origin and mechanism of production of UHECRs.

In the past 20 years, a number of experiments have gathered observations of UHECRs, and several papers have been written which look for such features in

²With the caveat that the time of propagation may depend on the energy and on the exact trajectory followed by the UHECR to reach us, making it possible that two particles reaching the Earth at different times have actually been emitted simultaneously.

the distribution of their directions of arrival, with sometimes contradictory conclusions. The difficulty lies in the fact that UHECRs are rare and that they do not arrive necessarily exactly from the direction where their source is located. Indeed, as typical cosmic ray particles are charged (which permits their acceleration by electromagnetic processes), they are deflected by Galactic and intergalactic magnetic fields. The deflection depends on the length of the path through the magnetic field and on the energy and charge of the particle. In fact, only very energetic cosmic rays (above few 10^{19} eV) with small charge (e.g., protons or nuclei with small atomic numbers) are expected to travel typical astrophysical distances from their source to us with deflection angles smaller than a few degrees. Details of the deflections are not known, as neither the exact magnitude, orientation and regularity on large scales of Galactic and extragalactic magnetic fields, nor the distance of the sources of UHECRs, nor the exact energy of the incoming cosmic ray, nor its charge (to within a factor of 26 between protons and iron nuclei), are known. Errors on the direction of the source of an UHECR can then be of order 1° at the lowest (typical error on the measurement of the direction of arrival with Auger), up to few degrees for protons, or tens of degrees for heavy nuclei travelling a long path through a regular galactic magnetic field.

Given a set of observed UHECRs, how can one best test for “repeaters” (cosmic rays coming from the same source) or, more generally, anisotropy in the distribution? If one restricts the analysis to the few events for which one is sure that the deflection angle is negligible, events are scarce and there are not enough statistics to conclude. As one selects events with less energy, the direction of origin becomes less reliable, with the total number of events completely dominated by those events with poorly constrained direction of origin. Finally, it is not clear how to build the isotropy test, without any sound prior knowledge about the uncertainty in the measured direction of the source. All of these are very meaningful questions to analyze UHECR observations.

Recently, an analysis of the direction of arrival of 27 UHECRs observed by the Pierre Auger experiment concludes in the existence of an anisotropy and a correlation with objects in a catalogue of nearby active galactic nuclei (AGNs), located at distances lower than about 70 Mpc^3 [Abraham et al. (2008)]. This anisotropy, however, is less obvious in a more recent analysis, based on 69 observed events [Pierre Auger Collaboration (2010)]. Clearly, the statistics are limited, and the development of new methods for investigating this topic can provide new insights on the origin of the UHECRs. Methods independent of external data sets such as the forementioned VCV catalogue (which is not a statistically well-characterized sample of AGNs but a compilation of published results) are of particular interest.

³70 million parsecs $\simeq 2.15 \times 10^{21}$ km.

1.2. *Outline of this work.* This work focuses on the important question of the isotropy of the cosmic rays. Because of the small number of available data, this question is not answered yet, although data from the Pierre Auger collaboration seems to hint at a correlation between the directions to the ultra-high energetic events (above 5.5×10^{19} eV) and the directions to active galactic nuclei in the catalogue compiled by Véron and Cetty-Véron [see [Pierre Auger Collaboration \(2008, 2010\)](#)]. From a statistical point of view, we address the question of testing the goodness of fit of the isotropy assumption to this small sample of directional data. The framework we choose is purely nonparametric, as we do not want to favour any particular alternative hypothesis, and as we wish to be able to discover unexpected forms of anisotropy.

The paper is organized as follows. In Section 2 we present a simplified model of cosmic ray propagation which will be used in Monte Carlo simulations to test the method. In Section 3 we present the nonparametric framework. Then we describe our needlet based anisotropy tests in Section 4. In Section 5 we present a Monte Carlo experiment that compares the power of the different tests and also the robustness of this power with respect to the parameters of the methods. We apply our procedures to real data from the Pierre Auger collaboration in Section 6. We then conclude and give perspectives for future extensions of the present work. An online supplement [[Faÿ et al. \(2013\)](#)] is devoted to a longer description of the type of wavelets we have used (the needlets) and the practical and numerical implementation of our methods. More numerical results are available there.

2. Simulating cosmic ray emission. In our investigation of tools to analyse the distribution of UHECR events, we need a way to simulate a distribution of observed events as a function of an underlying physical model. A complete Monte Carlo simulation of the physical processes of cosmic ray emission and propagation in the magnetic fields is beyond the scope of this paper and too dependent on a number of physical assumptions for which there is little available knowledge. We decide to perform qualitatively relevant simulations using a simple, although physically representative, toy model of cosmic ray emission and propagation.

2.1. *Cosmic ray sources.* In one hypothesis (H_0), we will assume that cosmic rays are emitted from a uniform distribution of many sources, that is, their directions of arrival are independent of the energy, and uniformly distributed on the celestial sphere. In the alternate hypothesis (H_1), we will assume that n cosmic rays originate from a small number n_s of sources, distributed uniformly in a spherical volume V of universe, of radius $r_{\max} = 70$ Mpc. For $n_s \gg n$, the distribution of directions of origin will be close to uniform and (H_1) indistinguishable from (H_0). For $n \gg n_s$, and n_s small, coincidences in the directions of arrival of the observed UHECRs will permit to identify easily the directions of the emitting sources. Our objective is to address the issue when n_s is comparable to the number of observed events n .

Simulations are performed as follows:

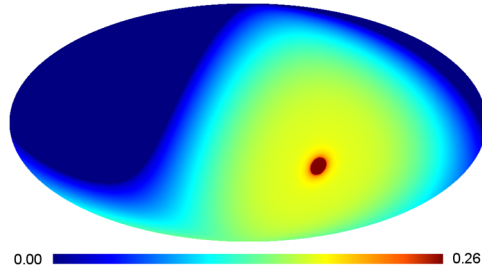


FIG. 1. Exposure function ε for the Pierre Auger Observatory in Galactic coordinates, represented through a Mollweide projection and computed from geometrical considerations [see Sommers (2001)]. The value of the exposure for some direction is defined as the probability that an incoming event from this direction is actually detected by the instrument. See Section 3.1.

- We fix the number n_s of sources and distribute them uniformly in the volume V . We assume that all sources are physically identical, that is, they emit cosmic rays with the same probability and the same distribution in energy, the latter coinciding with the observed flux dN/dE .
- We fix the number n of observed cosmic rays and draw at random their energies according to the distribution $n(E) \propto E^{-\alpha}$, $E \in [E_{\min}, E_{\max}]$, $\alpha > 0$.
- For each observed cosmic ray, we assign at random a corresponding emitting source, according to a probability density inversely proportional to the square of the distance D to the source (sources nearer produce a larger flux on Earth). This probability distribution can be modulated by the acceptance of the instrument for studying realistic test cases. For instance, Pierre Auger Collaboration (2010) uses 69 highest energy events for the search of correlations with astrophysical sources, selected by a cut in zenith angle of arrival ($\theta_{\text{zenith}} \leq 60^\circ$). Assuming homogeneous time coverage in UT over the years of observation, the exposure is computed straightforwardly from simple geometrical considerations [see Sommers (2001) and the details at the end of Section 2.2]. The map of Auger exposure computed in this way is displayed in Figure 1. The effect of the GZK cutoff is taken into account simply by limiting the volume to a sphere of 70 Mpc radius.
- For each cosmic ray, we modify the direction of arrival due to extragalactic magnetic fields. The next subsection describes the model used to implement these deflections.

2.2. *Deflection by Galactic and extragalactic magnetic fields.* Galactic magnetic fields are an important component of the Galactic interstellar medium (ISM). They can be probed in a variety of ways. The impact of local magnetic fields is observed in the optical wavelength range via starlight polarization. Indeed, elongated interstellar dust grains in the foreground of the observed star, aligned perpendicularly to magnetic field lines, absorb preferentially one direction of starlight

polarisation (along their major axis). Measurements of many stars reveal a general picture of the magnetic field in the Milky Way near the Sun [Heiles (1996), Fosalba et al. (2002)]. Aligned dust grains also emit polarized infrared emission, which can be used to infer magnetic fields in dust clouds [Benoît et al. (2004)]. Zeeman splitting of radio spectral lines allows for the direct measurement of relatively strong fields in nearby, dense gas clouds in the Milky Way [Crutcher et al. (2010)]. On larger-scales, the magnetic field of our Galaxy can be probed in three dimensions using Faraday rotation of pulsar signals [Han et al. (2006)]. Finally, synchrotron emission, emitted by relativistic electrons spiralling in the magnetic field, can be used to constrain the direction and amplitude of the magnetic field either from direct observation of the synchrotron polarisation [Page et al. (2007)] or by measuring the Faraday rotation of Galactic synchrotron using multi-wavelength observations in the radio range (below few GHz) [Beck (2011)].

In the vicinity of the Sun, the Galactic magnetic field has a typical amplitude of a few microGauss. This amplitude is typically increasing with decreasing distance toward the Galactic center, where it can reach values of a few tens of microGauss, and up to a few milliGauss in very local regions. In general, the regular component over most of the outer Galaxy is of the order of a few microGauss, aligned along the Galactic plane. The overall field structure follows the optical spiral arms, with evidence for at least one large-scale field reversal in the disk, inside the solar radius, and several distortions near star-forming regions.

For the purpose of estimating their impact on the deflection of high energy cosmic rays, Galactic magnetic fields are typically modeled as the sum of two components with different physical properties, a regular component and a turbulent component. The regular component roughly follows the spiral arms of the Galaxy and induces deflections typically perpendicular to the Galactic plane, that is, deflections in latitude of arrival. The turbulent component induces random deflections, which can be modeled as two-dimensional Gaussian distributions centered at the source. Indeed, we assume that such deflections are made of the superposition of many independent small deflections by independent regions with independent magnetic field directions, so that the Gaussian hypothesis is justified by the central limit theorem. We consider only cases in which the total deflection is small enough that the projection to the sphere is irrelevant (as well as the truncation of angles to 2π). Typical deflections for atomic nuclei are as follows [Harari, Mollerach and Roulet (2002)].

For the regular component (magnetic lensing effect),

$$(1) \quad \delta_{\text{reg}} = 3.25^\circ \left(\frac{10^{20} \text{ eV}}{E/Z} \right) \left(\frac{B}{2 \mu\text{G}} \right) \left(\frac{r}{3 \text{ kpc}} \right),$$

where E is the energy of the UHECR in eV, Z is the atomic number [e.g., 1 for hydrogen nuclei (protons), 2 for Helium nuclei (alpha particles), etc.], B is the magnetic field in microGauss (μG), and r the propagation length of the cosmic ray

in the magnetic field. The deflection is assumed deterministic (although energy-dependent), and the instantaneous direction of the deflection is along $\vec{v} \times \vec{B}$, where \vec{v} is the velocity of the incoming particle and \vec{B} the regular Galactic magnetic field, assumed to be along the y -axis of the Galactic coordinate system.

For the turbulent component (random deflection),

$$(2) \quad \delta_{\text{turb}} = 0.56^\circ \left(\frac{10^{20} \text{ eV}}{E/Z} \right) \left(\frac{B}{4 \mu\text{G}} \right) \sqrt{\frac{r}{3 \text{ kpc}}} \sqrt{\frac{L_{\text{gal}}}{50 \text{ pc}}}.$$

The deflection is Gaussian distributed with a standard deviation δ_{turb} and uniform distribution of the direction of the deviation in $[0, 2\pi[$. The deflections are written in terms of the typical expected values for the magnetic field ($2 \mu\text{G}$ for the regular part and $4 \mu\text{G}$ for the turbulent part), for coherence length L_{gal} of the turbulent part of the Galactic magnetic field (about 50 pc). 3 kpc is the typical propagation length r inside the Galactic magnetic field for a cosmic ray coming perpendicularly to the Galaxy. A plane parallel approximation of the disc-shaped geometry of the Milky Way suggests a dependence of r with the Galactic latitude b of the incoming cosmic ray. We assume here a dependence $r \propto 1/\sin b$, with a maximum length of 10 kpc, typical of the size of the Galactic disk.

Extragalactic magnetic fields also deflect cosmic rays originating from distant locations in the Universe. These deflections are expected to be qualitatively similar to those due to the turbulent part of the Galactic magnetic field, except that typical field strengths are smaller (and less well known) and correlation lengths are larger. Following The Pierre Auger collaboration [Pierre Auger Collaboration (2008)], we assume a deflection with standard deviation given by

$$(3) \quad \delta_{\text{ext}} = 2.4^\circ \left(\frac{10^{20} \text{ eV}}{E/Z} \right) \left(\frac{B}{1 \text{ nG}} \right) \sqrt{\frac{D}{100 \text{ Mpc}}} \sqrt{\frac{L_{\text{ext}}}{50 \text{ pc}}}.$$

UHECRs are observed to arrive on Earth with a flux dN/dE proportional to $E^{-4.2}$ for energies $E > 4 \times 10^{19}$ eV [Abraham et al. (2008)]. Although the shape of the spectrum is not very well constrained in this region (more recent Auger results suggest a spectral index closer to -4.3), the exact shape of the spectrum does not have a strong impact on the validity of our analysis. Our simulations will assume such a distribution, with various values for the minimum energy E_{min} and $E_{\text{max}} = 10^{21}$ eV. We focus on very energetic UHECRs ($E > 10^{19}$ eV) and assume UHECRs are light nuclei ($Z \approx 1$), for which deflections by magnetic fields are expected to be of the order of a few degrees.

We then implement cosmic ray deflections according to equation (3) (first the cosmic ray travels in the intergalactic medium) and then using both equations (1) and (2). As the exact nature of the cosmic rays has little impact on the general principles of our method, except that a change in atomic number induces a change in the scale of the deflections, we have assumed here for simplicity that all cosmic rays are protons (i.e., $Z = 1$). This, however, as a further refinement, can be easily

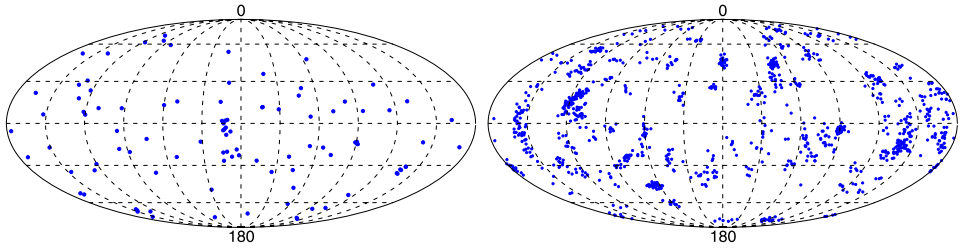


FIG. 2. Two simulations of the physical model described in Section 2, with $\alpha = 4.2$, $E_{\min} = 4 \times 10^{19}$, $E_{\max} = 10^{21}$. On the left, the number of sources is $n_s = 1000$ and the number of observations is $n = 100$. On the right, $n_s = 100$ and $n = 1000$. It appears in this latter case that clusters of events are of different typical angular size.

changed for practical application on real data sets. In particular, the presence or lack of anisotropy in the directions of arrival of the highest energy cosmic rays may help shed light on the nature of these particles, as iron nuclei, for instance, are more deflected by magnetic fields than protons, by a factor $Z_{\text{iron}} = 26$. This is an important point to take into account in view of recent Auger results that seem to indicate a low proton fraction at energy above 10^{18} eV, so that the cosmic rays at those energies might be essentially heavier nuclei [Abraham et al. (2010a)].

Figure 2 illustrates simulated outcomes in two extreme cases: few sources and many cosmic rays (right) and many sources and few cosmic rays (left).

In practice, instruments observe the sky unevenly. The capability of the instrument to observe in a particular direction of the sky depends on the field of view of the instrument and on the orientation of the instrument with respect to the sky (which itself depends on the sidereal time). From the properties of the instrument and the geometry of the observations, one can infer an equivalent observing time as a function of direction on the sky, that is, a function on the sphere that modulates the probability of detection of the observed cosmic rays. As an illustration, we have displayed on Figure 1 a Mollweide projection of the exposure map associated with the Pierre Auger Observatory, in Galactic coordinates, computed following Section 2 in Sommers (2001). This exposure map has been generated assuming a maximum accepted zenith angle for incoming cosmic rays of $\theta_{\text{zenith}} = 60^\circ$ and uniform distribution of observation periods in universal time (and hence, an exposure that depends exclusively of the declination, not the right ascension, in equatorial coordinates). The effect of the precession of equinoxes has been neglected for generating this exposure map (the perturbations it would generate are very tiny as compared to what we can measure with about 100 events, as currently available).

3. Nonparametric tests on the sphere.

3.1. *Introduction.* We assume that the cosmic rays arrive on Earth along a directional density h . We need to test

$$(T_1) \quad (H_0): h \equiv h_0 \quad \text{against} \quad (H_1): h \neq h_0,$$

where h_0 is the density under the null. For the above-mentioned reasons, we focus on test for anisotropy, then we choose $h_0 \equiv \frac{1}{4\pi}$. Note, however, that the whole subsequent setup can handle anisotropic choices for the null distribution. To take into account the nonuniform angular acceptance in the observation model, we model the exposure of the instrument by a known and arbitrary function $\varepsilon : \mathbb{S} \rightarrow [0, 1]$. In this setting, we assume that incoming events from direction $\xi \in \mathbb{S}$ have probability $\varepsilon(\xi)$ to be observed by the instrument. In this case, the observed incidental directions are distributed along a density f which is proportional to εh :

$$(4) \quad f(\xi) = \frac{\varepsilon(\xi)h(\xi)}{\int_{\mathbb{S}} \varepsilon(\xi')h(\xi') d\xi'}$$

Under the null, the observed directions of cosmic rays have a density

$$g(\xi) = \frac{\varepsilon(\xi)h_0(\xi)}{\int_{\mathbb{S}} \varepsilon(\xi')h_0(\xi') d\xi'}$$

Let (X_1, \dots, X_n) be an n sample of i.i.d. random positions on the two-dimensional sphere with probability density function f . In order to test for isotropy of the underlying physical phenomenon in this observational context, we need to implement the test

$$(\mathcal{T}_2) \quad (H_0) : f \equiv g \quad \text{against} \quad (H_1) : f \neq g.$$

On the real line, testing for $f \equiv g$ can be reformulated as testing for the uniform distribution of the sample $G(X_1), \dots, G(X_n)$ on $[0, 1]$, where G is the distribution function associated with the probability density g . For higher dimensions (as on the sphere), there is no natural transformation of the data, no notion of distribution function for directional data, that allows to recast (\mathcal{T}_2) as (\mathcal{T}_1) . Then we consider (\mathcal{T}_2) in its generality, with (\mathcal{T}_1) as a particular case.

Our aim in this paper is to provide test algorithms which are at the same time easy to implement, efficient in practical situations where the sample size is small (a few tens) and the data may be collected in a nonuniform or incomplete way, but also with properties that are likely to be optimal from a theoretical point of view.

Let us begin with a short review on nonparametric tests associated to function estimation, since this will inspire our study in many ways.

3.2. *Anisotropy tests among general nonparametric tests.* The test problem is well posed when the alternative is given. More often in practice it is wiser to consider a large nonparametric class of alternatives. To allow derivation of optimality properties, following standard point of view in a nonparametric framework [see, e.g., Ingster and Suslina (2003), Ingster (1993), Butucea and Tribouley (2006)], we shall consider smooth alternatives of the form

$$(5) \quad (H_{1,n}) : f \in \mathcal{F}_n(d, C),$$

where

$$(6) \quad \mathcal{F}_n(d, C) = \{g' \in \mathcal{R} : d(g'z, g) > Cr_n\}$$

and \mathcal{R} is a class of regularity, that contains, for example, all the twice continuously differentiable densities or densities satisfying the Hölder condition with Hölder exponent $s > 0$. We may consider balls in Sobolev or Besov spaces (see below). Here, d is a (semi-) distance between densities and r_n is referred to as a *separation rate*. Roughly speaking, d and r_n , respectively, define the shape and the size of the neighbourhood of the density under the null which is excluded from the alternative set of densities. The multiplicative constant C allows to define the concept of critical separation rate; see equations (9) and (10) below.

The choice of such alternatives is essential for the test procedure because the test statistics are built, more or less, on estimators of $d(f, g)$. For some particular distances, nonparametric estimators \hat{f} of the density of the observed sample may be plugged into the distance, namely,

$$\hat{d}(f, g) = d(\hat{f}, g).$$

For instance, \hat{f} could be a histogram-like (pixel-wise constant) density estimate of f based on counting events falling in any pixel of a given tessellation $\{V_k\}_{k=1, \dots, K}$ of the sphere, namely,

$$\hat{f} = \frac{1}{n} \sum_{k=1}^K \#\{X_i \in V_k, i = 1, \dots, n\} \frac{\mathbf{1}_{V_k}}{\mu(V_k)}$$

and the decision could be taken on the value of $d(\hat{f}, g) = \|\hat{f} - g\|^2$, say. Nevertheless, as described in Ingster (2000), such “plug-in” procedures are not always optimal in terms of rates of separation (see Section 4.2 for a more precise statement). In contrast, multiple tests have nice theoretical (minimax optimality and adaptivity) properties in various contexts: detection in a white noise model [Spokoiny (1996)], χ^2 test of uniformity on $[0, 1]$ [Ingster (2000)], goodness-of-fit test and model selection for random variables on the real line [Fromont and Laurent (2006)], two-sample homogeneity tests [Butucea and Tribouley (2006)], for instance. Note that one would also like to test for uniformity by taking into account the uncertainty on the measurements of the directional data. In a first approximation, this error can be modeled as a convolution noise: the observations are $Z_i = \varepsilon_i X_i, i = 1, \dots, n$, where $\varepsilon_1, \dots, \varepsilon_n$ is an i.i.d. sequence of random rotations in $\text{SO}(3)$. Lacour and Pham Ngoc (2012) addressed the problem of testing for the isotropy (X_1, \dots, X_n) in the particular case of a full-sky coverage with uniform exposure and from noisy observation (random rotations of the directions). As a consequence of the uniform coverage, their adaptive testing procedure is ideally constructed on the multipole moments of the observations.

If one has strong prior information, it is possible to construct tests that are not uniform except along a few set of directions, but which can have as much power

as possible at the $n^{-1/2}$ scale in those few directions of interest. This framework is introduced in [Bickel, Ritov and Stoker \(2006\)](#) and applied in [Bickel, Kleijn and Rice \(2008\)](#) for detecting periodicity in a sequence of photon arrival times. In our context, those directions are described by the Besov regularity of the alternative density, which is efficiently handled by the formalism of the wavelet analysis.

In the following paragraphs we discuss the various ingredients of our study.

3.2.1. *Distances.* We will consider standard distances of functions on the sphere, although there is in fact no clear choice for a 'good' distance in this framework: L^1 distance is generally more appropriate for probability densities, but L^p distances when p is increasing and especially L^∞ are more and more sensitive to bumps. As it is both usual and practical, we will mainly consider the L^2 distance (with respect to the invariant measure on the sphere). But, we will also consider expressing our results for other L^p distances such as L^1 and L^∞ . It is important to notice that it is the remarkable ability to concentrate the needlets that enables us to consider various distances. More traditional bases would only allow the L^2 distance and would then be much less sensitive to local changes.

3.2.2. *Separation rate.* Let $T(X_1, \dots, X_n) \in \{0, 1\}$ be a nonrandomized decision, that is, a measurable function of the sample (X_1, \dots, X_n) with value in $\{0, 1\}$. The dependence in n is omitted in most of our notation. As usual the event $[T = 1]$ is equivalent to the rejection of the null hypothesis. The probability of error of the first kind (false positive) of the decision is denoted

$$(7) \quad \alpha_n(T) = \mathbb{P}_g(T = 1),$$

while probability of error of the second kind (false negative) against the alternative (5) is

$$(8) \quad \beta_n(T, C) = \sup_{f \in \mathcal{F}_n(d, C)} \mathbb{P}_f(T = 0).$$

Here $\mathbb{P}_f, \mathbb{P}_g$ denote the probability measure under the density f or g for the i.i.d. sample (X_1, \dots, X_n) .

Formally, the separation rate is defined using the following minimax optimality criterion. A sequence r_n is a minimax rate of testing [see [Ingster \(2000\)](#)] if the following statements are satisfied:

1. For any r'_n such that $r'_n/r_n \rightarrow 0$ as $n \rightarrow \infty$,

$$(9) \quad \liminf_{n \rightarrow \infty} \inf_T \{\alpha_n(T) + \beta_n(T, 1)\} = 1,$$

where the infimum is taken on all decision rules, that is, $\{0, 1\}$ -valued measurable functions of the sample (X_1, \dots, X_n) .

2. For any $\alpha, \beta > 0$, there exist some constant $C > 0$ and a test statistic T^* (said *rate optimal in the minimax sense*), such that

$$(10) \quad \limsup_{n \rightarrow \infty} \alpha_n(T^*) \leq \alpha \quad \text{and} \quad \limsup_{n \rightarrow \infty} \beta_n(T^*, C) \leq \beta.$$

Condition (9) says that if the separation rate vanishes faster than r_n , then no test can do better than the blind random decision, for which the sum of the errors of the two kinds is exactly 1. Condition (10) says that there exists a decision that is efficient for such a separation rate, so that this rate is indeed a critical rate.

It is clear that a good test becomes sensitive to a closer and closer alternative hypothesis ($H_{1,n}$) when the sample size n grows. The notation of critical radius gives a precise and quantitative description of this behaviour. The rate $r_n = 1/\sqrt{n}$ is the usual rate in the regular parametric setting.

3.2.3. Invariance properties. As the uniform distribution is invariant under rotations of the sphere, the theory of invariant tests [see Lehmann and Romano (2005), Chapter 6] leads to impose the same kind of invariance on any statistical procedure for testing isotropy [see, e.g., Giné M. (1975) and the references therein]. As bases of invariant subspaces under rotations, the spherical harmonics are thus the most natural tools to detect some deviation from isotropy as in problem (\mathcal{T}_1). However, as explained earlier, a common property of astrophysical observation of (point or continuous) processes on the sphere is the nonuniform coverage of the *sky* by the instrument. It is common also that some parts of the data are missing or so noisy that it is preferable to completely ignore or mask them. That is why noninvariant approaches must be considered, and localized analysis functions (such as wavelets) may be used as alternatives to spherical harmonics. In the same spirit, wavelets have been proposed in the context of the angular power spectrum estimation by Baldi et al. (2009b) and used in the realistic case of a partially observed stationary process with heteroscedastic noise in Faÿ et al. (2008) and Faÿ and Guillaux (2011).

3.2.4. Regularity conditions: Besov spaces on the sphere. Although this is not directly the purpose of this paper, it is a natural question to ask which kind of regularity spaces our procedures are designed for. The problem of choosing appropriate spaces of regularity on the sphere is a serious question, and it is important to consider the spaces which generalize usual approximation properties. On the other hand, we are interested in spaces of functions which can be characterized by their needlet coefficients $\{\beta_{jk}\}$ associated to a needlet frame $\{\psi_{jk}\}$ (where j denotes the scale and k the position; see the online supplement [Faÿ et al. (2013)] for the precise definitions). Hence, as is standard in the nonparametric literature, it is natural to consider Besov bodies constructed on the needlet basis. In many situations (not only the sphere) it can be proved that these spaces can also be described as approximation spaces, so they have a genuine meaning and can be compared

to Sobolev spaces. We define here the Besov body B_{pq}^s as the space of functions $f = (4\pi)^{-1} \int_{\mathbb{S}} f \, d\mu + \sum_{j \geq 0} \sum_{k \in \mathcal{K}_j} \beta_{j,k} \psi_{j,k}$ such that

$$\sum_{j \geq 0} 2^{jsq} \left(\sum_{k \in \mathcal{K}_j} (|\beta_{j,k}| \|\psi_{j,k}\|_p)^p \right)^{q/p} < \infty$$

(with the obvious modifications for the cases p or $q = \infty$). Details on Besov spaces and their characterization by wavelets can be found in [Triebel \(1992\)](#) and [Meyer \(1992\)](#). For details on the relations between needlets and Besov spaces we refer, for instance, to [Narcowich, Petrushev and Ward \(2006a, 2006b\)](#), [Petrushev and Xu \(2008\)](#).

4. Needlet based test procedure and other anisotropy tests. We introduce here two anisotropy detection procedures based on the needlet analysis of $\{X_i\}_{i=1, \dots, n}$. The first one is based on multiple testing and will be referred to as MULTIPLE. The second one uses an estimate of the density plugged in a distance criterion and will be referred to as PLUGIN. For the sake of further comparison (see Section 5), we also describe two existing methods that are used in the gamma ray burst and cosmic ray literature. The first one is based on a nearest neighbour analysis [see [Quashnock and Lamb \(1993\)](#), [Efron and Petrosian \(1995\)](#)]. The second one relies on the two-point correlation [see, e.g., [Narayan and Piran \(1993\)](#), [Kachelriess and Semikoz \(2006\)](#)].

We want detection procedures that are efficient from a L^2 point of view, but also for other L^p norms. In addition, we will require procedures that are simple to implement as well as adaptive to unknown and inhomogeneous smoothness. In Euclidean frameworks, these types of requirements are well known to be efficiently handled by (nonlinear) wavelet thresholding estimation in the context of density estimation [see, e.g., [Donoho et al. \(1996\)](#)] or by multiple tests [[Ingster \(2000\)](#), [Spokoyny \(1996\)](#)].

Our problem here requires a special construction adapted to the sphere, since usual tensorized wavelets will never reflect the manifold structure of the sphere and will necessarily create unwanted artifacts. Recently a tight frame (i.e., a redundant family sharing some properties with orthonormal bases), called a *needlet frame*, was produced which enjoys enough properties to be successfully used for density estimation [[Baldi et al. \(2009a\)](#)], for example, concentration in the “Fourier” domain as well as in the space domain. Here, obviously the “space” domain is the two-dimensional sphere itself, whereas the Fourier domain is now obtained by replacing the “Fourier” basis by the basis of Spherical Harmonics which leads, as mentioned in the previous section, to invariant tests. This construction produces a family of functions $\{\psi_{jk}, j \geq 0, k \in \mathcal{K}_j\}$ which very much resemble wavelets. The index k defines (with an analogy to the standard wavelets) the *locations* (points) on the sphere around which the needlet is concentrated, and

j is referred to as the *scale*. These needlets have been shown to be extremely useful for solving several types of astrophysical problems [Delabrouille et al. (2009), Faÿ et al. (2008), Pietrobon, Balbi and Marinucci (2006), Marinucci et al. (2008), Pietrobon et al. (2008), Rudjord et al. (2009)] or diverse inverse problems in statistics [Kerkyacharian et al. (2007), Kerkyacharian, Pham Ngoc and Picard (2011), Kerkyacharian et al. (2010)]. They are especially well adapted to the situation recurrent in astrophysics where the “full sky” is not covered (meaning in our context that there are regions of the sphere where the points X_i are not observed if they happen to fall there).

A formal definition of needlets on the sphere is proposed in the online supplement to this article [Faÿ et al. (2013)] and can be found in greater detail in Narcowich, Petrushev and Ward (2006b). For the description of the test procedures, we only need to define the empirical needlet coefficients

$$(11) \quad \hat{\beta}_{jk} \stackrel{\text{def}}{=} \frac{1}{n} \sum_{i=1}^n \psi_{jk}(X_i),$$

which are unbiased estimators of $\beta_{jk}(f) \stackrel{\text{def}}{=} \langle f, \psi_{jk} \rangle = \int_{\mathbb{S}} f(\xi) \psi_{jk}(\xi) d\xi$. As usual in the wavelet literature, $j \geq 0$ refers to the scale and k to the location. The coarsest scale is $j = 0$. The index k refers to a collection of quadrature points $\{\xi_{j,k}\}$ that are available at each scale j . $\psi_{j,k}$ is then a zero-mean function centered on $\xi_{j,k}$ and more and more concentrated as $j \rightarrow \infty$.

In our simulations, we have chosen dyadic needlets with a spline function of order 15 as generator, which leads to simple but sufficiently concentrated analysis wavelets. All the wavelets are axisymmetric around some well chosen points $\xi_{j,k}$. The spatial profiles of those needlets at the five coarsest scales are represented in Figure 3. More details are available in the online supplement [Faÿ et al. (2013)].

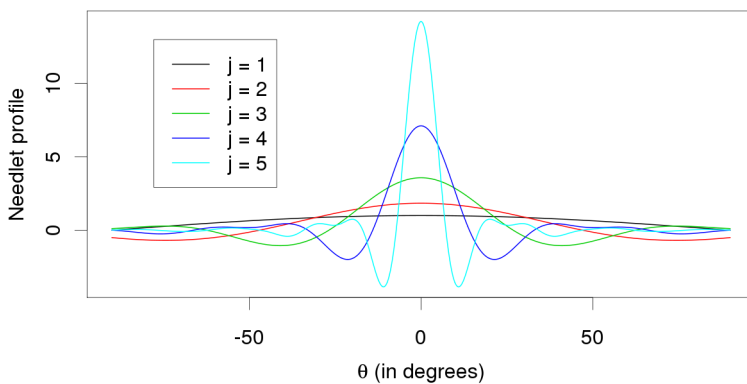


FIG. 3. The shape of the five first needlets in the spatial domain as the function of the co-latitude θ . Recall that all the $\psi_{j,k}$ functions are axisymmetric around the points $\xi_{j,k}$.

4.1. *Multiple tests.* For multiple tests, we will consider collections of “linear estimators” of the density, meaning that we will not use any nonlinear processing of wavelet coefficients such as thresholding in the estimation phase. By analogy with the work of Butucea and Tribouley (2006) on the related problem of the two-sample nonparametric homogeneity test, we define

$$(12) \quad \hat{f}_J = \frac{1}{4\pi} + \sum_{j=0}^J \sum_{k \in \mathcal{K}_j} \hat{\beta}_{jk} \psi_{jk}$$

with the β_{jk} ’s given by (11). For any value of the smoothing parameter J , we define the nonrandomized associated testing procedure

$$(13) \quad T_J = \mathbf{1}_{d(\hat{f}_J, g) \geq t_J} = \begin{cases} 1, & \text{if } d(\hat{f}_J, g) \geq t_J, \\ 0, & \text{if } d(\hat{f}_J, g) < t_J. \end{cases}$$

This gives a family of tests indexed by J , where the dependence with respect to the choice of the distance d and to the sequence of thresholds t_J is made implicit in the notation.

Butucea and Tribouley (2006) proved that if the regularity conditions are known and specified by Besov conditions, the smoothing parameter J can be chosen optimally. It is likely that their arguments could be reproduced in our case. However, our point of view in this paper will not be to detail this theoretical issue but rather to concentrate on the practical aspects of the tests. Moreover, it would be probably difficult to relate physical information to mathematical regularity conditions.

Nevertheless, the optimal choice for the parameter J depends on the regularity s specified in the class of alternatives. Adaptive optimality can be achieved thanks to a multiple test that decides for the alternative hypothesis as soon as one of the $T_J(d, c_J) = 1$ individually does so, that is, defining T^{MULTIPLE} , by

$$(14) \quad T^{\text{MULTIPLE}} = 0 \quad \text{if and only if} \quad \forall J \leq J^*, T_J = 0.$$

Mimicking the theoretical results obtained in Butucea and Tribouley (2006) and Baldi et al. (2009a), we have used

$$(15) \quad J^* = \lfloor \frac{1}{2} \log_2(n / \log n) \rfloor$$

as a reference in our numerical investigations, as in the case of adaptive density estimation (see below). Note, however, that the optimal J^* could vary according to the loss function (L^p norm) we use to measure the nonisotropy as suggested by the results of the related problem in the two sample nonhomogeneity detection Butucea and Tribouley (2006). The values t_J that are used in (13) must be chosen to verify $\mathbb{P}_g(T^{\text{MULTIPLE}} = 0) \simeq \alpha$, where α is the prescribed level of the test.

4.2. *Plug-in tests.* It is also interesting to compare, from an empirical point of view, the above multiple test procedures to algorithms where we simply plug in an adaptive estimate of the density in the distance. These density estimators have good asymptotic properties from a minimax point of view, hence, it makes sense to investigate also their properties when used for testing. To the best of our knowledge, no theoretical optimality is proved and there even are arguments suggesting that these procedures might not be optimal. For instance, on the real line, the minimax rate of convergence for estimation (in the so-called dense case) is $n^{-s/(2s+1)}$, meaning that if f belongs to a ball in a Hölder space with exponent s , then no estimator can approach the least favorable density at a better error rate (measured in a L^p norm). We refer to Donoho et al. [(1996), Theorem 3] for a precise statement, among others. On the other hand, the minimax critical radius for nonuniformity detection is $n^{-2s/(4s+1)}$ [see Ingster (2000)]. It means that, in the minimax framework, one can distinguish asymptotically two hypotheses that are separated by a distance negligible with respect to the accuracy of any nonparametric estimation of the densities in an infinite dimensional space.

The most popular minimax adaptive technique consists in adding to a very basic linear estimation a thresholding rule as post-processing. In the above mentioned paper [Baldi et al. (2009a)] this nonlinear post-processing actually is a *hard* thresholding rule, namely,

$$\hat{f}_{J^*} = \frac{1}{4\pi} + \sum_{j=0}^{J^*} \sum_{k \in \mathcal{K}_j} \hat{\beta}_{jk} \mathbf{1}_{|\hat{\beta}_{jk}| > \kappa \sqrt{\log n/n}} \psi_{jk}$$

for some positive constants κ and $J^* = \lfloor \frac{1}{2} \log_2(n/\log n) \rfloor$. The coefficients $\hat{\beta}_{jk}$ are defined in (11).

It is known that many variations exist with close theoretical properties but some differences in different practical situations. Among those, we will especially consider the data-driven thresholding introduced by Juditsky and Lambert-Lacroix (2004) to deal with density estimation on the real line (as opposed to density on $[0, 1]$). It seems to give good detection procedures for small samples in our context. In the following, we will consider the nonlinear estimates

$$(16) \quad \hat{f}_{J^*} = \frac{1}{4\pi} + \sum_{j=1}^{J^*} \sum_{k \in \mathcal{K}_j} \mathbf{1}_{|\hat{\beta}_{jk}| > \lambda \sqrt{\log n} \hat{\sigma}_{jk}} \mathbf{1}_{\delta_{jk} > \rho \log n} \hat{\beta}_{jk} \psi_{jk}$$

for some positive constants ρ, λ , $J^* = \lfloor \frac{1}{2} \log_2(n/\rho \log n) \rfloor$, and where

$$(17) \quad \hat{\sigma}_{jk}^2 \stackrel{\text{def}}{=} \frac{1}{n} \sum_{i=1}^n \psi_{jk}^2(X_i) - (\hat{\beta}_{jk})^2,$$

$$(18) \quad \delta_{jk} \stackrel{\text{def}}{=} (\psi_{jk}^2(\xi_{jk}))^{-1} \sum_{i=1}^n \psi_{jk}^2(X_i).$$

Let us give a short interpretation of the thresholding procedure. The quantity $\hat{\sigma}_{jk}^2$ is an estimate of the variance of $\hat{\beta}_{jk}$. The expression for δ_{jk} is inspired by the one provided in Juditsky and Lambert-Lacroix (2004). In this reference, compactly supported wavelets on the real line are used with a threshold on the number of observations actually participating to the estimation of β_{jk} . In this case, it makes sense to count the number of observations falling in the support of the wavelet. In our case, as needlets are supported on the whole sphere (although very concentrated), we propose to replace this quantity by a continuous type approximation δ_{jk} ; see (18). Note that $\delta_{jk} = n$ if $X_1 = \dots = X_n = \xi_{jk}$.

Finally, we define the PLUGIN procedure as the decision

$$(19) \quad T_J^{\text{PLUGIN}} = \mathbf{1}_{d(\hat{f}_{J^*}, g) \geq t_J^{\text{PLUGIN}}},$$

with \hat{f}_{J^*} defined in (16) and t_J^{PLUGIN} some fixed threshold depending on the prescribed level α of the test.

4.3. *Two-point correlation test and nearest neighbour test.* When dealing with one-dimensional data, one can compare every test procedure to the well-known benchmark Kolmogorov–Smirnov or Cramér–von Mises tests, which are based on the empirical distribution function of the sample. In higher dimensions (here on the sphere), there is no natural order relation that allows to consider such approaches. For sake of comparison, we have run some simulations on two different tests found in the astronomical literature.

Nearest neighbour test. The following statistical procedure has been proposed by Quashnock and Lamb (1993). We denote it NN, as nearest neighbour. For each point X_i , we compute the distance Y_i to its nearest neighbour. Under the hypothesis that f is uniform over the whole sphere, the marginal distribution function of (Y_i) is $\phi : y \mapsto 1 - [(1 + \cos y)/2]^{n-1}$, and the Wilcoxon statistic

$$W = \sqrt{12n} \left(\frac{1}{2} - \frac{1}{n} \sum_{i=1}^n \phi(Y_i) \right)$$

is asymptotically standard Gaussian. For a nonhomogeneous random draw (for instance, in the presence of clusters), this statistic is expected to take significantly high values, allowing to detect this kind of anisotropy. This test is of interest, as it is simple to compute, it has no parameters to be tuned, and it admits an extension to nonuniform exposure [see Efron and Petrosian (1995)]. In this case, the distribution of W is estimated numerically by Monte Carlo methods. The NN procedure simply writes

$$(20) \quad T^{\text{NN}} = \mathbf{1}_{W \geq t^{\text{NN}}},$$

where $t_{1-\alpha}^{\text{NN}}$ is the $(1 - \alpha)$ -quantile of the distribution of W . This distribution can be approximated by a standard Gaussian distribution if the sample size is big and the exposure is uniform. Otherwise, the quantile is estimated by the Monte Carlo method.

Two-point correlation test. Among others, [Kachelriess and Semikoz \(2006\)](#), [Narayan and Piran \(1993\)](#) use the empirical two-point autocorrelation function to detect clustering (TWOPC test). For a collection of n points $\{X_i\}$ and any angular distance $\delta \in [0, \pi]$, let $N_n(\delta)$ denote the random number of pairs $\{i, j\}$ such that $\Delta(X_i, X_j) \leq \delta$, where Δ is the geodesic distance. Define the two-point correlation function $w_n(\delta) = \mathbb{E}(N_n(\delta))$ and its empirical counterpart

$$(21) \quad \hat{w}_n(\delta) = \sum_{i < j} \mathbf{1}_{[0, \delta]}(\Delta(X_i, X_j)).$$

Under the null hypothesis, the distribution of \hat{w}_n at any δ_0 is evaluated using Monte Carlo simulations. Then, the detection will be based on the comparison between the empirical correlation function and w_n , at some fixed value δ_0 or a few different values. A typical δ_0 can be chosen so as to maximize the sensitivity of the test depending on the application. In some references, however, the probability to observe a value bigger than $\hat{w}_n(\delta)$ is plotted on the whole range $[0, \pi]$ with no δ_0 fixed a priori. Consequently, much care is taken when interpreting those values, as stressed, for instance, in [Kachelriess and Semikoz \(2006\)](#). Here we define the procedure TWOPC by the decision

$$(22) \quad T^{\text{TwoPC}} = \mathbf{1}_{\hat{w}_n(\delta_0) \geq t^{\text{TwoPC}}},$$

where $t_{1-\alpha}^{\text{TwoPC}}$ is the $(1 - \alpha)$ quantile of the distribution of $\hat{w}_n(\delta_0)$ under the null, evaluated by Monte Carlo simulations, at some δ_0 specified a priori.

5. Monte Carlo experiments.

5.1. Experimental setup. In this section we compare numerically the tests defined in Section 4 that are denoted MULTIPLE, PLUGIN, NN and TWOPC.

For T being any of those nonrandomized test procedures, we can tune the parameters of the procedure to have a prescribed level α , that is, $\mathbb{P}_g(T = 1) = \alpha$. This is done by Monte Carlo replication. Ten thousand independent random samples of size n are drawn under the null hypothesis, for g being the uniform density on \mathbb{S} [i.e., $g \equiv 1/(4\pi)$] or the stylized exposure function of the Pierre Auger detector (see Figure 1).

For the MULTIPLE procedure and a given level α , we have chosen

$$(23) \quad T_j = \mathbf{1}_{\|\hat{f}_j - g\|_p > t_{\alpha', j}},$$

where $t_{\alpha', j}$ is the $1 - \alpha'$ quantile of the distribution of $\|\hat{f}_j - g\|_p$ under the null hypothesis. This distribution is evaluated using Monte Carlo replications. Further, the value α' is chosen so that

$$(24) \quad T'_{j^*} = \sup_{j=1, \dots, J^*} T_j$$

TABLE 1
 Power (in %) under (H_1^c) , under uniform exposure, with $n_s = 100$ and $E_{\min} = 10^{19}$ eV

		<i>n</i> = 25				<i>n</i> = 100			
<i>J</i> [★]		3	4	5	6	3	4	5	6
MULTIPLE	<i>p</i> = 1	51	46	41	40	98	98	98	98
	<i>p</i> = 2 [★]	52	53	47	47	98	99	98	98
	<i>p</i> = ∞	42	44	42	42	92	91	91	90
PLUGIN	<i>p</i> = 1	34	34	34	34	98	98	98	98
	<i>p</i> = 2	42	42	42	42	98	98	98	98
	<i>p</i> = ∞	50	50	50	50	92	92	92	92
NN				38				82	
TWOPC				45				62	

has a first type error probability equal to α . This is arbitrary and the theory to be written would likely suggest to use a scale dependent level.

The power of the test *T* is defined by (8). Some clues about this value are obtained by evaluating $\mathbb{P}_f(T = 1)$ for particular alternatives *f* that are given in the next section. Here again, those quantities are evaluated by Monte Carlo. Note, however, that the power for a particular alternative only gives an upper bound of the power in the minimax sense given by the second equation of (8).

In the tables of tests in the main paper (Tables 1 through 3) and on its online supplement [Tables 1 through 8 in Faÿ et al. (2013)], we represent the power of four tests. The power of the needlet tests is expressed as a function of the finest band *J*[★] and the power of the norm we use to detect anisotropy (see the online supplement [Faÿ et al. (2013)] for more details on the actual implementation of the method).

TABLE 2
 Power (in %) under (H_1^c) , under uniform exposure, with $n_s = 500$ and $E_{\min} = 6 \times 10^{19}$ eV

		<i>n</i> = 25				<i>n</i> = 100			
<i>J</i> [★]		3	4	5	6	3	4	5	6
MULTIPLE	<i>p</i> = 1	27	39	45	43	76	94	99	98
	<i>p</i> = 2 [★]	28	42	50	58	79	96	100	100
	<i>p</i> = ∞	24	35	45	50	69	84	96	97
PLUGIN	<i>p</i> = 1	18	18	18	18	72	72	73	73
	<i>p</i> = 2	25	28	29	29	78	82	82	82
	<i>p</i> = ∞	33	34	34	34	71	80	80	80
NN				33				99	
TWOPC				75				99	

TABLE 3

Power of the tests for three models of (H_1^a) with values of δ and sample size varying so that $\sqrt{nd}(f, g)$ remains constant. It appears that those particular sequences of powers are generally nondecreasing with the sample size. The observation model uses the Pierre Auger exposure function

J^*		$n = 25, \delta = 0.08$				$n = 100, \delta = 0.04$				$n = 400, \delta = 0.02$			
		3	4	5	6	3	4	5	6	3	4	5	6
MULTIPLE	$p = 1$	14	16	13	13	14	16	14	14	21	20	17	17
	$p = 2^*$	19	20	16	16	17	21	20	20	23	21	20	20
	$p = \infty$	23	26	23	22	29	32	32	30	34	32	30	29
PLUGIN	$p = 1$	11	11	11	11	17	16	16	16	19	19	19	19
	$p = 2$	16	16	16	16	26	27	27	27	32	32	32	32
	$p = \infty$	23	22	22	22	32	30	30	30	39	39	39	39
NN			8			6				5			
TwoPC			35			14				14			

The profile cuts of the (axisymmetric) needlets we have used are plotted in the online supplement.

5.2. *Alternatives.* We have investigated the performance of the test (power against level) for sample sets of small to moderate size ($n = 25, 100, 400$) and against different alternatives. Those choices of n mimic the progressive publication of events by the Pierre Auger Observatory (27 events above 5.7×10^{19} eV in 2008, 69 above 5.5×10^{19} in 2010, a few hundred in the future).

Generally speaking, the physical plausibility of those alternatives is weak [alternative (H_1^c)], if not null [alternatives (H_1^b) and (H_1^c)]. Our goal is to focus here on specific departures from isotropy. First we consider unimodal nonisotropic densities, with a Gaussian shape. Then we consider mixtures of densities that would only be obtained if the sources of the cosmic rays were known to be uniformly distributed and repeating, and at the same distance from us. Third, the Physics-inspired model (H_1^c) gives rise to nonisotropic patterns with richer frequency content compared to the previous ones (and nonaxisymmetric clusters). We now give the precise definitions of the alternatives.

(H_1^a) . The first family of alternatives is obtained as a mixture of the uniform density h_0 and an over-density at some point of the sphere, with Gaussian-like axisymmetric profile. Precisely, the density under (H_1^a) writes

$$h(\xi) = (1 - \delta)h_0 + \delta h_\theta(\xi),$$

where for $\theta \neq 0$, we put $h_\theta(\xi) := h_{\theta, \xi_0}(\xi)$, $h_{\theta, \xi_0} := C_\theta \exp(-(\xi \cdot \xi_0)^2 / 2\theta^2)$ and $\xi_0 = (\pi/2, 0)$. Such densities are then unimodal, with a bump whose width is proportional to θ . Typical observations of random draw with such density with $\delta = 0.01$ and $\theta = 5^\circ$ or 20° are displayed on Figure 4.

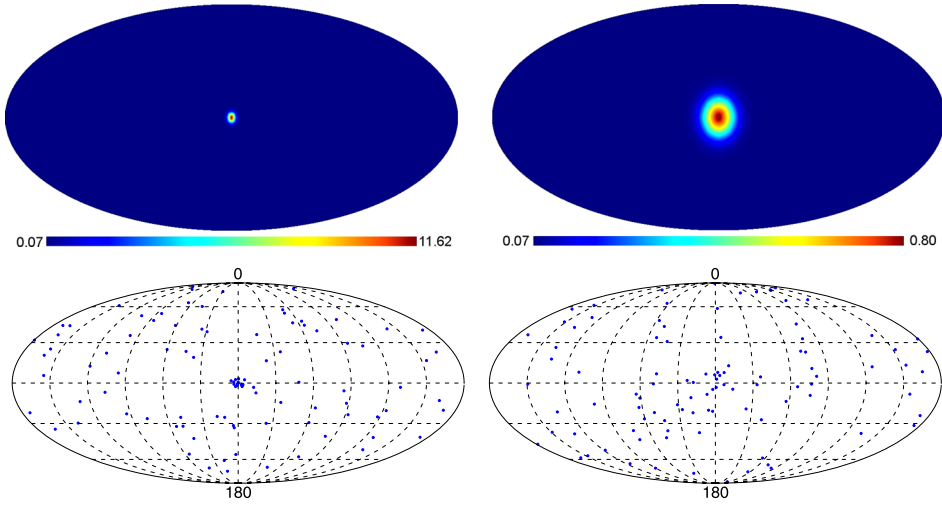


FIG. 4. Densities (first line) and random draws (second line, $n = 100$) under (H_1^a) with $\delta = 10\%$ and $\theta = 5^\circ$ (left) or $\theta = 20^\circ$ (right).

(H_1^b) . A second family of alternatives is a toy model for the repeating emission of events from a small number of sources, as explained in the Introduction. Here we assume that the n_s sources are uniformly distributed, although in a realistic case, we can expect any type of astrophysical sources to follow the local matter density of the cosmic structure (which would make the detection of anisotropy easier). This generalization is straightforward enough that we do not discuss it further at this stage. Conditionally to those positions, the incidental directions are distributed along a mixture of n_s Gaussian densities centred on the sources (to take into account the error in the measurement of the incidence angle or the deflection of the charged particle by Galactic magnetic fields), namely,

$$h(\xi) = \sum_{j=1}^{n_s} h_{\theta, \xi_j}(\xi).$$

This density is then modulated by the exposure ε of the detector along equation (4). Such conditional densities are displayed on the first line of Figure 5 with uniform and Pierre Auger exposures. We considered the cases $n_s = 10$ and $n_s = 100$ and fixed $\theta = 10^\circ$. Note that if n_s is much bigger than n , it is difficult to detect this kind of anisotropy (which can be detected only if at least one source has emitted more than one cosmic ray).

(H_1^c) . A third and last alternative is obtained by the physical model of cosmic ray observations described in detail in Section 2. Sources are randomly drawn in a spherical volume of radius $r_{\max} = 70$ Mpc, and their flux is assumed inversely proportional to the square of their distance. The parameters for the simulations

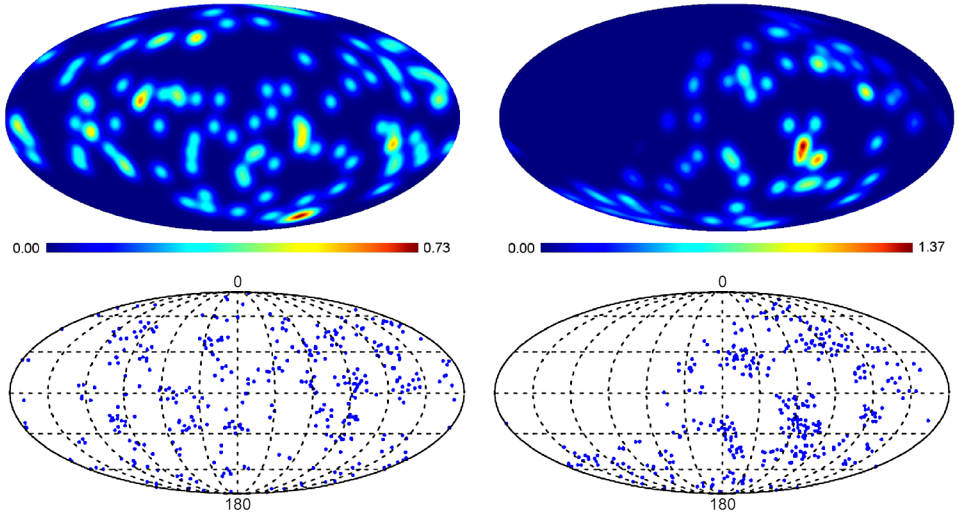


FIG. 5. Density of X_1 conditionally to the random draw of the centers of 100 AGNs (first line) and random draws with $n = 400$ (second line). The exposure is uniform on the left, à la Pierre Auger Observatory on the right.

are taken to be $E_{\max} = 10^{21}$ eV, $\alpha = 4.2$. We consider different values for E_{\min} (namely, 1, 4 or 6×10^{19} eV). Playing on this parameter has an important practical incidence. Assuming that the distribution of the energy of the cosmic rays is a power law, $\mathbb{P}(E > t) \sim Ct^{-\alpha+1}$, lowering the threshold on the selection of the cosmic rays from 6×10^{19} eV to 4×10^{19} eV (resp., 10^{19} eV) accounts to increase the size of the sample (available observations above the threshold) by a factor $(6/4)^{\alpha-1} \simeq 3.66$ (resp., 310). It means that the statistical decision should be made far easier if the cosmic rays were not too much isotropized by the Galactic fields as their energies go lower. This effect is illustrated in Figure 6. It is interesting to see if the methods are still able to detect anisotropy as the cosmic rays become more and more isotropized. This is a more realistic simulation compared to models (H_1^a) and (H_1^b) . There is no single size for the scatter of the CRs coming for a given source, nor the same size or directionality for each source, nor the same flux for

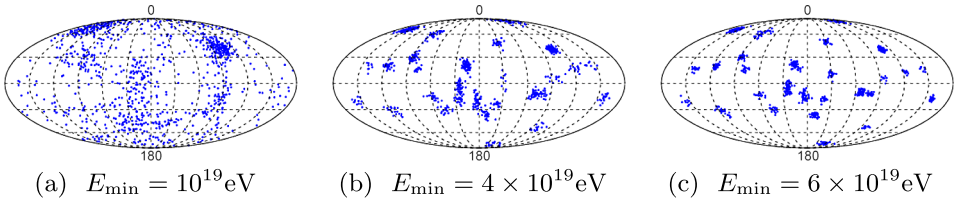


FIG. 6. Isotropization of the cosmic rays in model (H_1^c) as E_{\min} decreases. There are the exact same $n_s = 30$ sources in the three cases and $n = 1000$ observations.

each source, that hence is interesting specifically for a multiscale analysis with no prior assumption about a correlation length.

Note that under the alternatives (H_1^b) and (H_1^c) , the procedure is to be understood as a test on the conditional distribution of $(X_i)_{i=1,\dots,n}$ with respect to the positions of the “sources”, which are randomly drawn once for all.

5.3. Numerical results and discussion.

Tables. We shall represent some of the results of our simulations with tables of estimated power of the procedures for given alternatives (in percent), at the prescribed level $\alpha = 0.05$. Practically, we let the finest needlet band entering the MULTIPLE and PLUGIN procedures vary in the set $\{J^* - 2, J^* - 1, J^*, J^* + 1\}$ where J^* is given by (15). The entry (or entries) corresponding to the overall highest power (before rounding off) among the 26 values is (are) printed in bold type. We consider three L^p norms, namely, L^p for $p = 1, 2, \infty$. It is possible to use an unbiased estimate of the distance between \hat{f} and g in the case of the L^2 norm. It is referred to as $p = 2^*$ (see the online supplement for details)

ROC curves. The receiver operating characteristic (ROC) curves plot the power p of a procedure as a function of its level α . It is a useful representation for comparison of different procedures along a wide range of levels. The ROC curves associated to the TWOPC procedure are a step function because of the discrete nature of the test statistic. Some of the ROC curves are nonconcave. It should be recalled, however, that any procedure of this kind can be improved to a randomized procedure whose ROC curve is the concave upper envelope of the original one. Accordingly, the reader’s eyes must actually analyse the upper envelopes of the ROC curves. Note that the power in the tables has not been modified by this argument.

ROC curves are represented in plots with four subplots, corresponding to the four above-mentioned choices of J^* in the needlet methods. The ROC curves for TWOPC and NN procedures are the same in the four subplots. Inset graphs allow complementary comparison of the methods by zooming on the most relevant levels (small α).

5.3.1. *Some specific results.* First, we note that the differences of sensitivity between the different L^p norms we use are not very strong, probably because we consider quite regular alternative hypotheses. As expected, the L^∞ is a bit more sensitive to more spiky (unimodal) distributions, whereas more global measures such as L^1 or L^2 perform better under the (H_1^b) or (H_1^c) models. This is illustrated by some ROC curves in the online supplement. We now illustrate the comparison of the performances of the four procedure with a few tables and figures.

It appears that the methods MULTIPLE and PLUGIN have a consistent behaviour when the typical radius of the anisotropic structure is varying. We shall discuss

further from those cases below. Figure 7 illustrates their good performances even for small samples under the model (H_1^c) that produce clusters of various sizes and shapes.

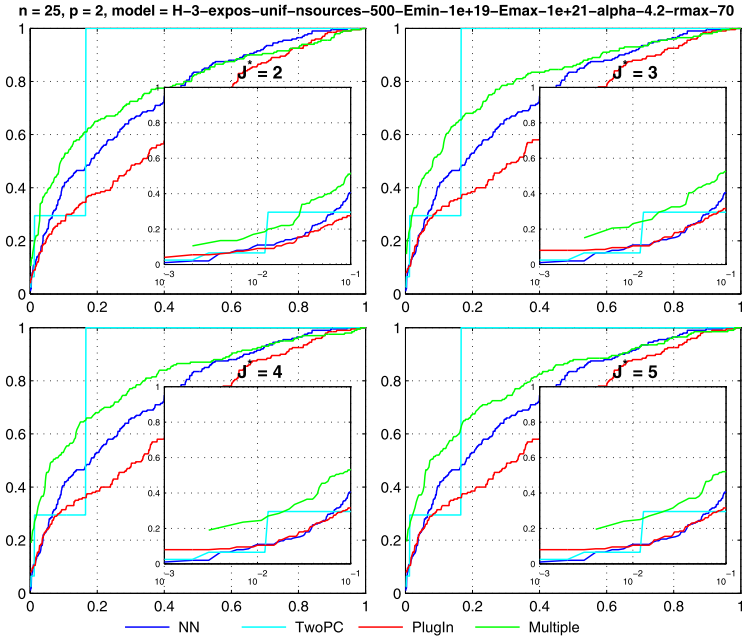
The NN procedure performs strikingly worse than others in almost all but the (H_1^b) situations. The good sensitivity to (H_1^b) alternatives can be explained in the following manner. In this case, the points $\{X_i\}_{i=1,\dots,n}$ are mainly grouped into clusters of average scale given by the standard deviation of the Gaussians of the mixture. If the number of clusters and this standard deviation are too small to cover significantly the whole observed part of the sphere, then the random distances to the nearest neighbour are bounded by σ with very high probability, which is not the case under the null. This makes the distribution of the distance to the nearest neighbour a very sensitive tool to discriminate between (H_1^b) and the null.

Varying the alternatives, it appears that no method outperforms the other in a uniform way, but it seems that the two needlet methods, if not always optimal, consistently have a good behaviour. Moreover, the MULTIPLE test is slightly more sensitive than the PLUGIN one. As an illustration, we represent in Tables 1 and 2 the power of the procedures against the (H_1^c) alternative, for sample sizes equal to 25 and 100, and $(E_{\min}, n_s) = (10^{19} \text{ eV}, 100)$, and $(6 \times 10^{19} \text{ eV}, 500)$, respectively. It can be seen from those tables that moving the lower energy limit upwards makes the detection easier. More tables are available in the online supplement, for a representative panel of alternatives, containing more or less spiky distributions, clusters of smoother alternatives, weak or strong anisotropy etc.

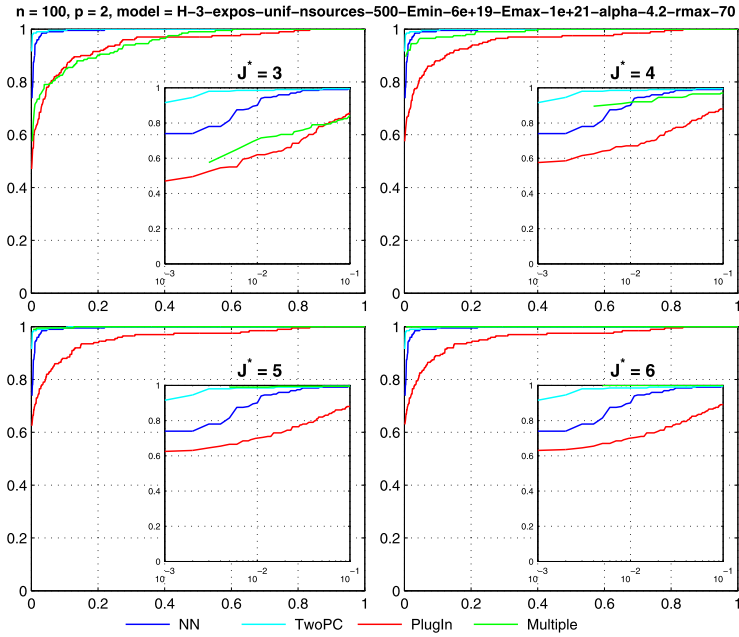
It must be stressed that the TWOPC approach often provides a good sensitivity if not the best at $n = 25$. For most of the alternatives, however, one or the other of the needlets methods outperforms TWOPC as n grows. This is exemplified in Tables 1 and 2 in the case of a (H_1^c) alternative. In our application context, the sample size over a given energy threshold is increasing with time and experiments, so it must be highlighted that multiscale methods are more and more appropriate for analysis of future data sets.

5.3.2. Separation rate. We focus here on the behaviour of the power of the test with respect to n . If r_n is the critical rate in the minimax sense [given by equations (9) and (10)], we should observe an approximately same power for different sample size and the least favourable alternative densities \tilde{f}_n as soon as the quantity $r_n d(\tilde{f}_n, g)$ remains constant.

On Table 3 we have displayed the power of the different procedures for three different densities corresponding to the alternative (H_1^a) and three sample sizes, keeping the same value for $n^{1/2}d(f, g)$. Indeed, in the (H_1^a) case, for any power norm, $d(h, h_0) = \delta d(h_0, h_\theta)$. As the power remains roughly the same in $(0, 1)$ for the three values of the parameters, and as $n^{1/2}$ is an upper bound for the minimax separation rate in analogy with similar problems on Euclidean spaces, this numerical simulation is consistent with the claim that the needlet based procedures perform well at the minimax rate of testing. The increasing value of the power with n



(a) $n = 25$



(b) $n = 100$

FIG. 7. ROC curves (true positive rate against false positive rate) for the four methods. For the needlet methods, the debiased L^2 norm is used. Insets display the same curves as in the main plot with a logarithmic scale in abscissas, to highlight the comparative performances for relevant level values.

together with the unbeatable rate of separation \sqrt{n} illustrates the fact that we only have access to upper bounds of the minimax rate. In other words, the densities under consideration are definitely not the least favourable cases. The comparison of needlet methods with NN and TWOPC methods tends to be more favourable to needlets methods as n becomes larger in this case.

5.3.3. Robustness. Assume that the anisotropy detection by the needlet methods is adaptive. Then, as pre-tuned black boxes, those methods should remain optimal on a wide range of alternatives. Some simulations support this claim. Note, however, that we only explore physically possible alternatives which are smooth nonuniform densities.

The key parameter of the TWOPC method is the angular size δ_0 at which we compare $\hat{w}(\delta)$ to the distribution of $w(\delta_0)$ under the null. For sake of fairness in our comparisons, we should allow some tuning of this parameter. It is clear that the optimal δ_0 is related to the “average scale” of the anisotropy. Though it is difficult to give a precise and general definition of this former quantity, it should be close to the value of the parameter θ in the particular case of model (H_1^a) . Indeed, it appears from our simulations that TWOPC is better than the needlet methods when $\theta = 5^\circ$ and worse when $\theta = 20^\circ$ under (H_1^a) .

On Figure 8 we have plotted the estimated power of the tests against different alternatives (H_1^a) or (H_1^c) , and for different parameters for the methods. In the case of (H_1^a) , the first line of the figure shows that the optimal δ_0 is indeed related to the parameters θ of the alternative. However, when dealing with alternatives such as (H_1^c) (second line of Figure 8) that give rise to structures at different “scales”, the optimal choice of δ_0 is not clear. By observing the large variations of the power of the TWOPC procedure with respect to δ_0 in both cases, one can conclude that this procedure should incorporate a data-driven selection of δ_0 to be truly efficient.

The situation is strikingly different for the needlet methods. One can observe from the left column of Figure 8 that the power reaches some *plateau* after $J^* > J_{\min}$ in a very consistent way across the different alternatives. This robustness is a strong point of those methods. The dependence in n is quite weak too. For instance, taking $J^* = 4$ leads to a small loss of efficiency uniformly with respect to the best choice for each given situation of sample size and model.

6. Analysis of Auger data. We have run the previous tests on the Auger public data made available by the [Pierre Auger Collaboration \(2010\)](#). It is composed of 69 arrival directions of cosmic rays with energy above 55 EeV and detected by the Pierre Auger Observatory between 1 January 2004 and 31 December 2009. Those directional events are plotted on Figure 9. The distributions of the tests under study for $n = 69$ and under the null hypothesis have been evaluated by Monte Carlo simulation of length 10.000.

Along with the detection of a correlation between cosmic rays’ directions and catalogues of potential sources, the Pierre Auger collaboration already performed

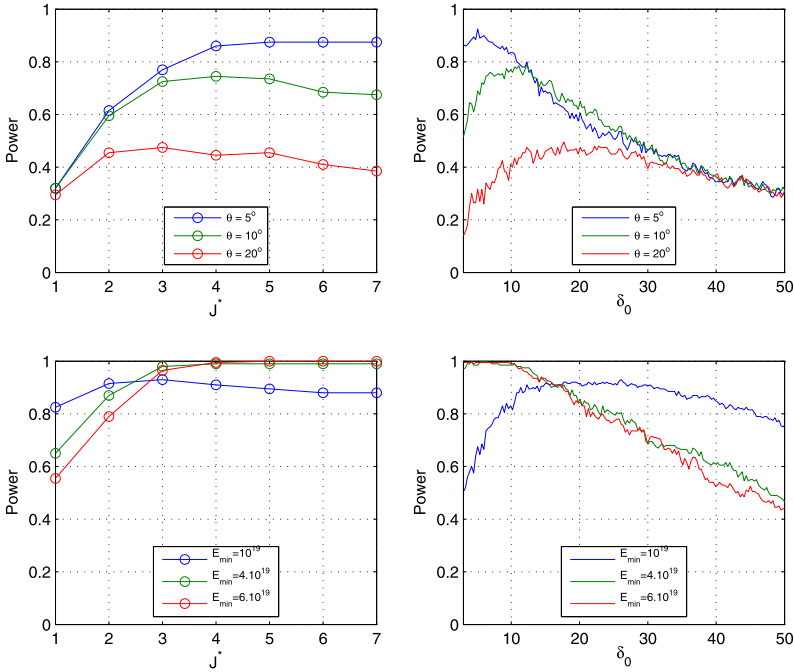


FIG. 8. The empirical power associated with the MULTIPLE (left column) and TWOPC (right column) procedures with respect to their key parameters J^* and δ_0 , respectively. The prescribed levels of the tests are 5%. The three models under consideration in the first row are provided by the alternative (H_1^a) with $\theta = 5^\circ, 10^\circ$ and 20° . On the second row, the three alternative models are (H_1^c) with $n_s = 500$, and $E_{\min} = 10^{19}, 4 \times 10^{19}$ or 6×10^{19} eV. The number of observations is $n = 100$ everywhere.

a catalogue-free test for anisotropy with no reference to any catalogue, using the TWOPC procedure. As noticed earlier, the critical value for this method is the choice of δ_0 in (22). The p -value of this test for the 69 UHECRs data set reaches a minimal value of

$$p\text{-value(TWOPC)} \simeq 0.008$$

around $\delta_0 \simeq 10.7^\circ$. Recall that in order to be interpretable as a classical p -value for a single hypothesis testing, this p -value should be computed from an out-of-the-sample prescription of δ_0 , which is not the case here. Then this p -value strongly exaggerates the significance of the detection. Indeed, as already noticed in [Pierre Auger Collaboration (2010)], we computed that the fraction of isotropic simulations that are as nonisotropic as the real data at some angle between 4° and 14° is as high as 10%. We have also computed that

$$p\text{-value(NN)} \simeq 0.07.$$

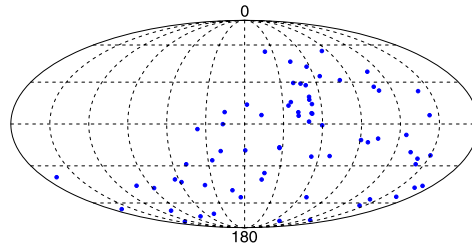


FIG. 9. The 69 arrival directions of cosmic rays with energy above 55 EeV and detected by the Pierre Auger Observatory up to 31 December 2009 [Pierre Auger Collaboration (2010)]. Their distribution is obviously nonuniform, due to the incomplete coverage function of the instrument that is described in Figure 1. Anisotropy tests actually compare the empirical distribution to the exposure function (see text for details).

The p -values of Table 4 are the p -values computed from the Pierre Auger data set for our MULTIPLE and PLUGIN procedure.

For the MULTIPLE test, the p -value is defined as the proportion of draws (under the null) that have a higher single test statistic in at least one value of $j \in \{1, \dots, J^*\}$. The resulting p -value is quite sensitive to the choice of the highest band J^* , except if one uses the L^2 -norm. Note that if we take the L^2 norm and the theoretical $J^* = 2$ given by the expression (15), the results for the MULTIPLE test are not statistically significant. But the Monte Carlo simulations suggest that this theoretical choice of J^* is not optimal for small to medium sample size, being too small.

The PLUGIN is more stable and consistently considers that the Auger data is significantly nonisotropic. The almost constant p -values in this case are the consequence of a hard thresholding rule in (16) that cancels all the estimated coefficients $\hat{\beta}_{j,k}$ as soon as $j \geq 3$ for this data set. This may in turn give a rule-of-thumb rule to define a data-driven J^* for the multiple test.

To conclude on this important data set and this methodology, it appears that the needlet methods find a stronger statistical evidence of some kind of anisotropy in

TABLE 4
P-values of the MULTIPLE and the PLUGIN tests for Auger data ($n = 69$)

J^*	MULTIPLE test			PLUGIN test		
	$p = 1$	$p = 2^*$	$p = \infty$	$p = 1$	$p = 2^*$	$p = \infty$
1	0.957	0.788	0.387	0.956	0.958	0.397
2	0.051	0.112	0.035	0.033	0.037	0.036
3	0.118	0.050	0.004	0.017	0.008	0.005
4	0.434	0.046	0.003	0.017	0.008	0.008
5	0.227	0.095	0.624	0.017	0.008	0.008
6	0.762	0.045	0.341	0.017	0.008	0.008

the Pierre Auger data. More realistic alternatives and more simulations can help to choose the J^* parameter of the MULTIPLE procedure and additional parameters of the PLUGIN approach.

7. Conclusion. In this paper we have investigated the problem of the detection of anisotropy of directional data on the unit sphere, with an application to the analysis of ultrahigh energy cosmic ray events as observed with a detector such as the Pierre Auger Observatory. It was important to consider samples whose sizes are comparable to the sizes of the data sets that are available nowadays for cosmic rays scientists (about 25 at the beginning of this work, about a hundred now). Although we are mainly interested in small sample performances, we have proposed a multiple test approach based on a multiresolution analysis of the data, which could hopefully be proved to be asymptotically optimal in the minimax sense, a well-known pessimistic framework.

We have proposed, and tested on various simulated data sets, two methods using the decomposition of the directional data onto a frame of spherical needlets. Their performance has been compared to other (more specific) approaches based on the nearest neighbour and on the two-point correlation function. The simulation shows that the needlet-based methods perform comparatively very well in various situations. They are competitive with the existing method at a small sample size, and tend to outperform them from a moderate sample size. Moreover, the “omnibus” property of the needlets method is interesting for the problem at hand, in which the type of possible anisotropy (the class of alternative) is not really well known a priori. In addition, a multiple test based on the use of spherical needlets offers a good opportunity to extend the method of detection of anisotropies with not only multiplicity in the scales tested, but also in ranges of energy of the incoming particles. Indeed, while in this work we have used the energy level as a simple threshold, one could instead implement a detection using the joint directional-energy information—allowing thus to simultaneously extract information from the highest energy cosmic rays, which are not deflected much by Galactic and extragalactic magnetic fields, and also from lower energy events, more deflected but much more numerous. In light of our simulations on an energy level-dependent model, the multiscale approach could lead to stronger conclusion using the CR data that are not yet made public by the Pierre Auger Observatory.

As in any nonparametric method, there is at least one parameter to be tuned, often by hand or using more sophisticated data-driven methods such as cross-validation. In the needlet methods one can tune several parameters (shape of the needlets, highest scale J^* — although there is an asymptotic formula for it, thresholds on the coefficients in the PLUGIN approaches, thresholds on the individual tests in the MULTIPLE procedure, power norm). It is plausible, however, that a large range of possible choices for most of these parameters give comparable performance.

Although we have used needlets that are compactly supported windows in the harmonic space, it may be arguable that they are not the most appropriate tool. One could consider, as an alternative, better spatially concentrated functions [see, e.g., Lan and Marinucci (2009), such as the Mexican needlets] or, in general, try to optimize the needlet window function given prior knowledge of the physical problem and of the expected properties of anisotropic distributions of the cosmic ray direction of incidence. In this spirit, it would be interesting to consider directional wavelet such as curvelets or ridgelets [see Starck et al. (2006)] to test for specific strip-like alternative densities. It is also possible to consider nondyadic needlets. The choice of $\mathcal{B} \in (1, 2)$ allows a finer coverage of the frequency line. The numerical results presented here have not taken this benefit into full account, and whether significantly higher power can be obtained by optimizing this number remains to be investigated.

Finally, in addition to the aforementioned possible extensions of our methods, we want to stress that the work presented here also opens the way to two lines of future investigations, one on the applications side and one more theoretical. On the experimental side, it will be of much interest to apply the method on larger data sets (for instance, by lowering the energy threshold to increase the available sample size). On the theoretical side, the validation of the approach has to be investigated on the basis of some theory in the minimax framework it is designed for.

Acknowledgments. For the numerical part of this work, we acknowledge the use of the HEALPix package [Górski et al. (2005)] and of the SphereLab (an OCTAVE interface to HEALPix package, needlet transforms and utilities). We thank Dmitri Semikoz for useful discussions concerning high energy cosmic rays, and Maude le Jeune, Jean-François Cardoso and Frédéric Guilloux for making available some of the tools used for the computational aspects of the present work. We thank the anonymous referees and Associate Editor for their suggestions and remarks that significantly improved the presentation of this paper.

SUPPLEMENTARY MATERIAL

Supplement to “Testing the isotropy of high energy cosmic rays with spherical needlets” (DOI: [10.1214/12-AOAS619SUPP](https://doi.org/10.1214/12-AOAS619SUPP); .pdf). In the supplement, we recall the construction of the needlet decomposition on the sphere, and discuss its practical usage. We also complete the Section 5 of this paper with more results obtained from Monte-Carlo simulations.

REFERENCES

- ABRAHAM, J. et al. (2008). Observation of the suppression of the flux of cosmic rays above 4×10^{19} eV. *Phys. Rev. Lett.* **101** 061101.
- ABRAHAM, J. et al. (2010a). Measurement of the depth of maximum of extensive air showers above 10^{18} eV. *Phys. Rev. Lett.* **104** 091101.

- ABRAHAM, J. et al. (2010b). Measurement of the energy spectrum of cosmic rays above 10^{18} eV using the Pierre Auger observatory. *Phys. Lett. B* **685** 239–246.
- BALDI, P., KERKYACHARIAN, G., MARINUCCI, D. and PICARD, D. (2009a). Adaptive density estimation for directional data using needles. *Ann. Statist.* **37** 3362–3395. [MR2549563](#)
- BALDI, P., KERKYACHARIAN, G., MARINUCCI, D. and PICARD, D. (2009b). Asymptotics for spherical needles. *Ann. Statist.* **37** 1150–1171. [MR2509070](#)
- BECK, R. (2011). Cosmic magnetic fields: Observations and prospects. In *American Institute of Physics Conference Series* (F. A. Aharonian, W. Hofmann and F. M. Rieger, eds.) **1381** 117–136. American Institute of Physics, Melville, NY.
- BENOÎT, A. et al. (2004). First detection of polarization of the submillimetre diffuse galactic dust emission by Archeops. *Astron. Astrophys.* **424** 571–582.
- BHATTACHARJEE, P. and SIGL, G. (2000). Origin and propagation of extremely high energy cosmic rays. *Phys. Rep.* **327** 109–247.
- BICKEL, P., KLEIJN, B. and RICE, J. (2008). Event-weighted tests for detecting periodicity in photon arrival times. *Astrophysical Journal* **685** 384–389.
- BICKEL, P. J., RITOV, Y. and STOKER, T. M. (2006). Tailor-made tests for goodness of fit to semi-parametric hypotheses. *Ann. Statist.* **34** 721–741. [MR2281882](#)
- BUTUCEA, C. and TRIBOULEY, K. (2006). Nonparametric homogeneity tests. *J. Statist. Plann. Inference* **136** 597–639. [MR2181971](#)
- CRONIN, J. W. (2005). The highest-energy cosmic rays. *Nuclear Physics B Proceedings Supplements* **138** 465–491.
- CRUTCHER, R. M., WANDEL, B., HEILES, C., FALGARONE, E. and TROLAND, T. H. (2010). Magnetic fields in interstellar clouds from Zeeman observations: Inference of total field strengths by Bayesian analysis. *Astrophysical Journal* **725** 466–479.
- DELABROUILLE, J., CARDOSO, J. F., LE JEUNE, M., BETOULE, M., FAÏ, G. and GUILLOUX, F. (2009). A full sky, low foreground, high resolution CMB map from WMAP. *Astronomy and Astrophysics* **493** 835–857.
- DONOHO, D. L., JOHNSTONE, I. M., KERKYACHARIAN, G. and PICARD, D. (1996). Density estimation by wavelet thresholding. *Ann. Statist.* **24** 508–539. [MR1394974](#)
- EFRON, B. and PETROSIAN, V. (1995). Testing isotropy versus clustering of Gamma-Ray bursts. *Astrophysical Journal* **449** 216.
- FAÏ, G. and GUILLOUX, F. (2011). Spectral estimation on the sphere with needles: High frequency asymptotics. *Stat. Inference Stoch. Process.* **14** 47–71. [MR2780648](#)
- FAÏ, G., DELABROUILLE, J., KERKYACHARIAN, G. and PICARD, D. (2013). Supplement to “Testing the isotropy of high energy cosmic rays using spherical needles.” DOI:10.1214/12-AOAS619SUPP.
- FAÏ, G., GUILLOUX, F., BETOULE, M., CARDOSO, J. F., DELABROUILLE, J. and LE JEUNE, M. (2008). CMB power spectrum estimation using wavelets. *Phys. Rev. D* **78** 083013.
- FOSALBA, P., LAZARIAN, A., PRUNET, S. and TAUBER, J. A. (2002). Statistical properties of galactic starlight polarization. *Astrophysical Journal* **564** 762–772.
- FROMONT, M. and LAURENT, B. (2006). Adaptive goodness-of-fit tests in a density model. *Ann. Statist.* **34** 680–720. [MR2281881](#)
- GINÉ M., E. (1975). Invariant tests for uniformity on compact Riemannian manifolds based on Sobolev norms. *Ann. Statist.* **3** 1243–1266. [MR0388663](#)
- GÓRSKI, K., HIVON, E., BANDAY, A., WANDEL, B., HANSEN, F., REINECKE, M. and BARTELMANN, M. (2005). HEALPix: A framework for high-resolution discretization and fast analysis of data distributed on the sphere. *Astrophysical Journal* **622** 759–771.
- GREISEN, K. (1966). End to the cosmic-ray spectrum? *Phys. Rev. Lett.* **16** 748–750.
- HAN, J. L., MANCHESTER, R. N., LYNE, A. G., QIAO, G. J. and VAN STRATEN, W. (2006). Pulsar rotation measures and the large-scale structure of the galactic magnetic field. *Astrophysical Journal* **642** 868–881.

- HARARI, D., MOLLERACH, S. and ROULET, E. (2002). Astrophysical magnetic field reconstruction and spectroscopy with ultra high energy cosmic rays. *J. High Energy Phys.* **7** 6.
- HEILES, C. (1996). A comprehensive view of the galactic magnetic field, especially near the Sun. In *Polarimetry of the Interstellar Medium* (W. G. Roberge and D. C. B. Whittet, eds.). *Astronomical Society of the Pacific Conference Series* **97** 457. Astronomical Society of the Pacific, San Francisco, CA.
- HILLAS, A. M. (1984). The origin of ultra-high-energy cosmic rays. *Annual Review of Astronomy and Astrophysics* **22** 425–444.
- INGSTER, Y. I. (1993). Asymptotically minimax hypothesis testing for nonparametric alternatives. I. *Math. Methods Statist.* **2** 85–114. [MR1257978](#)
- INGSTER, Y. I. (2000). Adaptive chi-square tests. *J. Math. Sciences* **99** 1110–1120.
- INGSTER, Y. I. and SUSLINA, I. A. (2003). *Nonparametric Goodness-of-fit Testing Under Gaussian Models. Lecture Notes in Statistics* **169**. Springer, New York. [MR1991446](#)
- JUDITSKY, A. and LAMBERT-LACROIX, S. (2004). On minimax density estimation on \mathbb{R} . *Bernoulli* **10** 187–220. [MR2046772](#)
- KACHELRIESS, M. and SEMIKOZ, D. V. (2006). Clustering of ultra-high energy cosmic ray arrival directions on medium scales. *Astroparticle Physics* **26** 10–15.
- KERKYACHARIAN, G., PHAM NGOC, T. M. and PICARD, D. (2011). Localized spherical deconvolution. *Ann. Statist.* **39** 1042–1068. [MR2816347](#)
- KERKYACHARIAN, G., PETRUSHEV, P., PICARD, D. and WILLER, T. (2007). Needle algorithms for estimation in inverse problems. *Electron. J. Stat.* **1** 30–76. [MR2312145](#)
- KERKYACHARIAN, G., KYRIAZIS, G., LE PENNEC, E., PETRUSHEV, P. and PICARD, D. (2010). Inversion of noisy Radon transform by SVD based needlets. *Appl. Comput. Harmon. Anal.* **28** 24–45. [MR2563258](#)
- KOTERA, K. and OLINTO, A. V. (2011). The astrophysics of ultrahigh-energy cosmic rays. *Annual Review of Astron and Astrophys* **49** 119–153.
- LACOUR, C. and PHAM NGOC, T. M. (2012). Goodness-of-fit test for noisy directional data. Available at [arXiv:1203.2008](#).
- LAN, X. and MARINUCCI, D. (2009). On the dependence structure of wavelet coefficients for spherical random fields. *Stochastic Process. Appl.* **119** 3749–3766. [MR2568294](#)
- LEHMANN, E. L. and ROMANO, J. P. (2005). *Testing Statistical Hypotheses*, 3rd ed. Springer, New York. [MR2135927](#)
- MARINUCCI, D., PIETROBON, D., BALBI, A., BALDI, P., CABELLA, P., KERKYACHARIAN, G., NATOLI, P., PICARD, D. and VITTORIO, N. (2008). Spherical needlets for CMB data analysis. *Monthly Notices of the Royal Astronomical Society* **383** 539–545.
- MARTÍNEZ, V. J. and SAAR, E. (2002). *Statistics of the galaxy distribution*. Chapman & Hall/CRC Press, Boca Raton, FL.
- MEYER, Y. (1992). *Wavelets and Operators. Cambridge Studies in Advanced Mathematics* **37**. Cambridge Univ. Press, Cambridge. Translated from the 1990 French original by D. H. Salinger. [MR1228209](#)
- NARAYAN, R. and PIRAN, T. (1993). Do gamma-ray burst sources repeat? *Monthly Notices of the Royal Astronomical Society* **265** L65–L68.
- NARCOWICH, F., PETRUSHEV, P. and WARD, J. (2006a). Decomposition of Besov and Triebel–Lizorkin spaces on the sphere. *J. Funct. Anal.* **238** 530–564. [MR2253732](#)
- NARCOWICH, F. J., PETRUSHEV, P. and WARD, J. D. (2006b). Localized tight frames on spheres. *SIAM J. Math. Anal.* **38** 574–594 (electronic). [MR2237162](#)
- PAGE, L. et al. (2007). Three-year Wilkinson Microwave Anisotropy Probe (WMAP) observations: Polarization analysis. *Astrophysical Journal Supplement* **170** 335–376.
- PETRUSHEV, P. and XU, Y. (2008). Localized polynomial frames on the ball. *Constr. Approx.* **27** 121–148. [MR2336420](#)

- PIERRE AUGER COLLABORATION (ABRAHAM, J. et al.) (2008). Correlation of the highest-energy cosmic rays with the positions of nearby active galactic nuclei. *Astroparticle Physics* **29** 188–204.
- PIERRE AUGER COLLABORATION (ABRAHAM, J. et al.) (2009). Upper limit on the cosmic-ray photon fraction at EeV energies from the Pierre Auger observatory. *Astroparticle Physics* **31** 399–406.
- PIERRE AUGER COLLABORATION (ABREU, P. et al.) (2010). Update on the correlation of the highest energy cosmic rays with nearby extragalactic matter. *Astroparticle Physics* **34** 314–326.
- PIETROBON, D., BALBI, A. and MARINUCCI, D. (2006). Integrated Sachs–Wolfe effect from the cross correlation of WMAP3 year and the NRAO VLA sky survey data: New results and constraints on dark energy. *Phys. Rev. D* **74** 043524.
- PIETROBON, D., AMBLARD, A., BALBI, A., CABELLA, P., COORAY, A. and MARINUCCI, D. (2008). Needlet detection of features in the WMAP CMB sky and the impact on anisotropies and hemispherical asymmetries. *Phys. Rev. D* **78** 103504.
- QUASHNOCK, J. M. and LAMB, D. Q. (1993). Evidence for the Galactic origin of gamma-ray bursts. *Monthly Notices of the Royal Astronomical Society* **265** L45–L50.
- RUDJORD, Ø., HANSEN, F. K., LAN, X., LIGUORI, M., MARINUCCI, D. and MATARRESE, S. (2009). An estimate of the primordial non-Gaussianity parameter f_{NL} using the needlet bispectrum from WMAP. *Astrophysical Journal* **701** 369–376.
- SOMMERS, P. (2001). Cosmic ray anisotropy analysis with a full-sky observatory. *Astroparticle Physics* **14** 271–286.
- SPOKOINY, V. G. (1996). Adaptive hypothesis testing using wavelets. *Ann. Statist.* **24** 2477–2498. [MR1425962](#)
- STARCK, J. L., MOUDDEN, Y., ABRIAL, P. and NGUYEN, M. (2006). Wavelets, ridgelets and curvelets on the sphere. *Astronomy and Astrophysics* **446** 1191–1204.
- TORRES, D. F. and ANCHORDOQUI, L. A. (2004). Astrophysical origins of ultrahigh energy cosmic rays. *Rep. Progr. Phys.* **67** 1663–1730.
- TRIEBEL, H. (1992). *Theory of Function Spaces. II. Monographs in Mathematics* **84**. Birkhäuser, Basel. [MR1163193](#)
- ZATSEPIN, G. T. and KUZ’MIN, V. A. (1966). Upper limit of the spectrum of cosmic rays. *Soviet Journal of Experimental and Theoretical Physics Letters* **4** 78.

G. FAY
 LABORATOIRE MAS
 ECOLE CENTRALE PARIS
 GRANDE VOIE DES VIGNES
 92 295 CHÂTENAY-MALABRY
 FRANCE
 E-MAIL: gilles.fay@ecp.fr

G. KERKYACHARIAN
 UNIVERSITÉ PARIS X-NANTERRE
 CNRS LPMA
 175 RUE DU CHEVALERET
 75013 PARIS
 FRANCE
 E-MAIL: kerk@math.jussieu.fr

J. DELABROUILLE
 LABORATOIRE APC, CNRS UMR7164
 10 RUE A. DOMON ET L. DUQUET
 75013 PARIS
 FRANCE
 E-MAIL: delabrouille@apc.univ-paris7.fr

D. PICARD
 UNIVERSITÉ PARIS DIDEROT
 CNRS LPMA
 175 RUE DU CHEVALERET
 75013 PARIS
 FRANCE
 E-MAIL: picard@math.jussieu.fr